Supplementary Information (SI) for Inorganic Chemistry Frontiers.
This journal is © the Partner Organisations 2025

Electronic Supplementary Information

Salt-protected carbonization of a metal–organic framework for enhanced nitrogen doping and high porosity leading to efficient performance in oxygen reduction reaction

*Ahram Yoo, Sujeong Lee, Sojin Oh, Songhee Kim and Moonhyun Oh**

Department of Chemistry, Yonsei University, 50 Yonsei-ro, Seodaemun-gu, Seoul 03722, South Korea
*Corresponding author.
E-mail: moh@yonsei.ac.kr

Materials and Characterizations

Zinc(II) nitrate hexahydrate ($Zn(NO_3)_2 \cdot 6H_2O$, 98%), 1,4-benzenedicarboxylic acid (H_2BDC, 98%), *N,N*-dimethylacetamide (DMA, 99%), urea (99.0–100.5%), sodium chloride (NaCl, ≥99.5%), 20 wt% platinum on graphitized carbon (Pt/C), and 5 wt% Nafion solution were purchased from Sigma-Aldrich. Methylene chloride (98%) and ethyl alcohol (99.5%) were purchased from SAMCHUN. Deionized water was obtained from Millipore Direct-Q3. All pellet samples were prepared using an MTI Corporation YLJ-24TS hydraulic press. Scanning electron microscopy (SEM) images were acquired using a JEOL IT-500HR field-emission SEM instrument (Yonsei Center for Research Facilities, Yonsei University). Elemental mapping images were acquired using a JEOL JSM-IT500HR field-emission SEM equipped with a JEOL EX-74600U4L2Q energy-dispersive X-ray spectroscopy (EDX) detector. Powder X-ray diffraction (PXRD) patterns were obtained using a Rigaku MiniFlex 600 instrument equipped with a Cu Kα radiation source (40 kV, 15 mA). Energy-dispersive X-ray (EDX) spectra were obtained using a Hitachi SU 1510 SEM equipped with a Horiba EMAX Energy E-250 EDX system. The N_2 adsorption–desorption isotherms (77 K) were measured using a BELSORP Max volumetric adsorption equipment system. All isotherms were obtained after pretreatment under a dynamic vacuum at 25 °C for 3 h, except in the case of MOF-5. MOF-5 was analyzed after pretreatment under a dynamic vacuum at 300 °C for 3 h. Raman spectra were acquired using a Raman spectrometer (HORIBA Jobin Yvon LabRAM ARAMIS) at room temperature with a 0.5 mW YAG laser (532 nm). X-ray photoelectron spectroscopy (XPS) analysis was conducted using a Thermo Scientific K-Alpha KA1066 spectrometer with a monochromatic Al Kα X-ray source ($h\nu$ = 1486.6 eV). The XPS profiles were calibrated using the measured C 1s peak position at 284.6 eV.

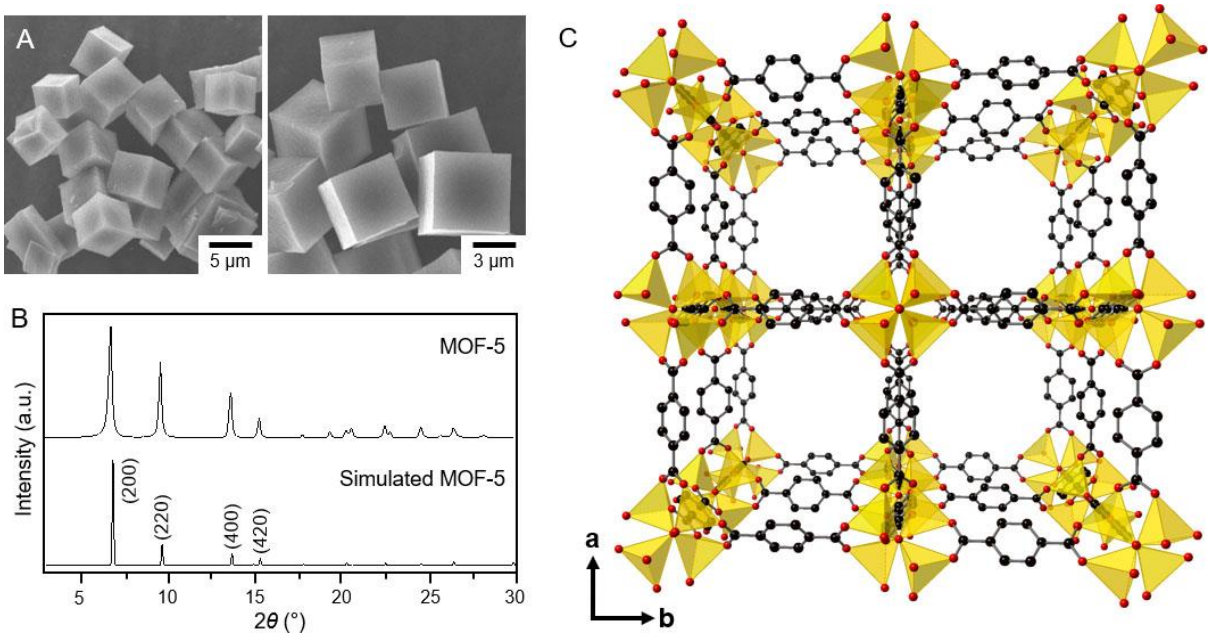

Fig. S1 (A) SEM images of MOF-5. (B) PXRD pattern of MOF-5 with the simulated PXRD pattern included for reference. Ball-and-stick representation of MOF-5, depicting carbon (black), oxygen (red), and zinc (dark yellow) atoms. Hydrogen atoms are omitted for clarity. [Cambridge Crystallographic Data Centre (CCDC) 938392].[1]

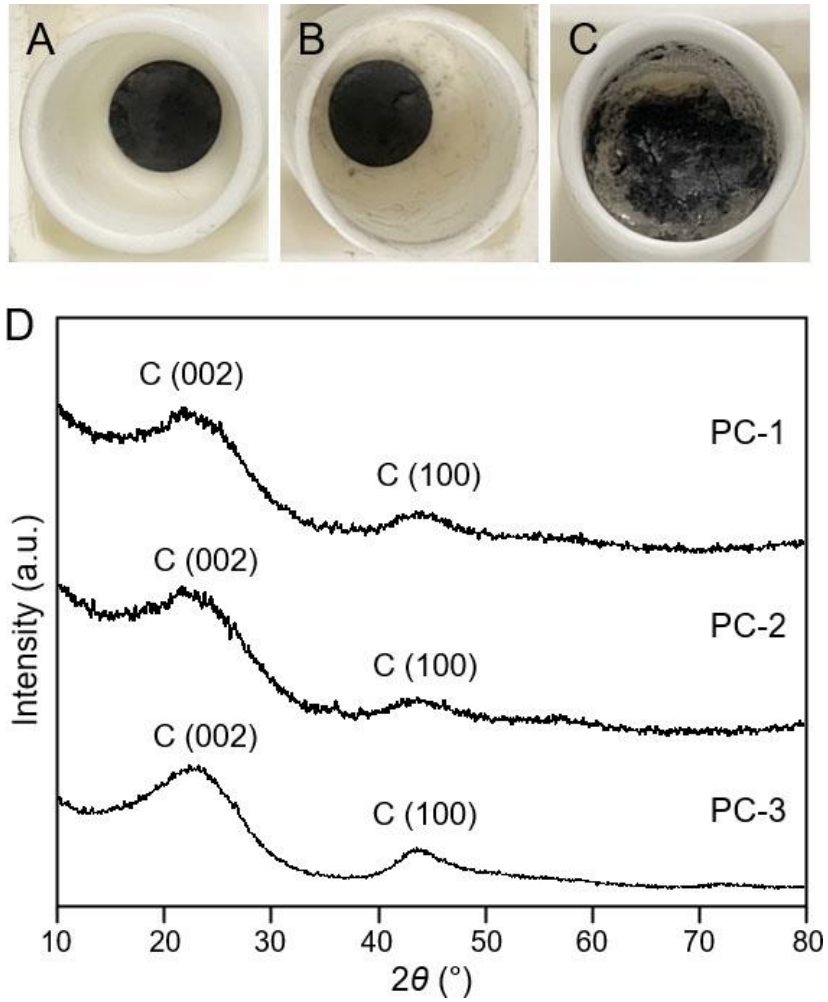

Fig. S2 Photographs of pellets of (A) MOF-5, (B) MOF-5/urea, and (C) MOF-5/urea@NaCl after pyrolysis at 950 °C for 3 h. (D) PXRD patterns of PC-1–PC-3.

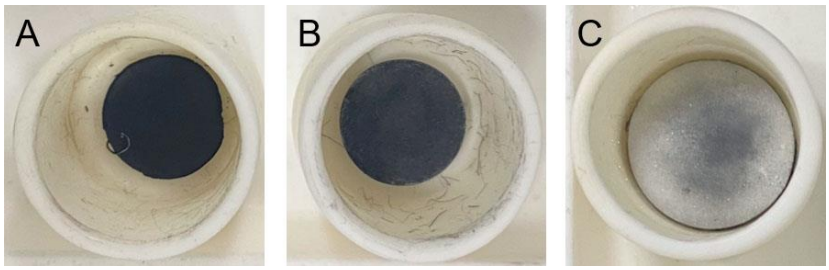

Fig. S3 Photographs of pellets of (A) MOF-5, (B) MOF-5/urea, and (C) MOF-5/urea@NaCl after pyrolysis at 800 °C for 3 h.

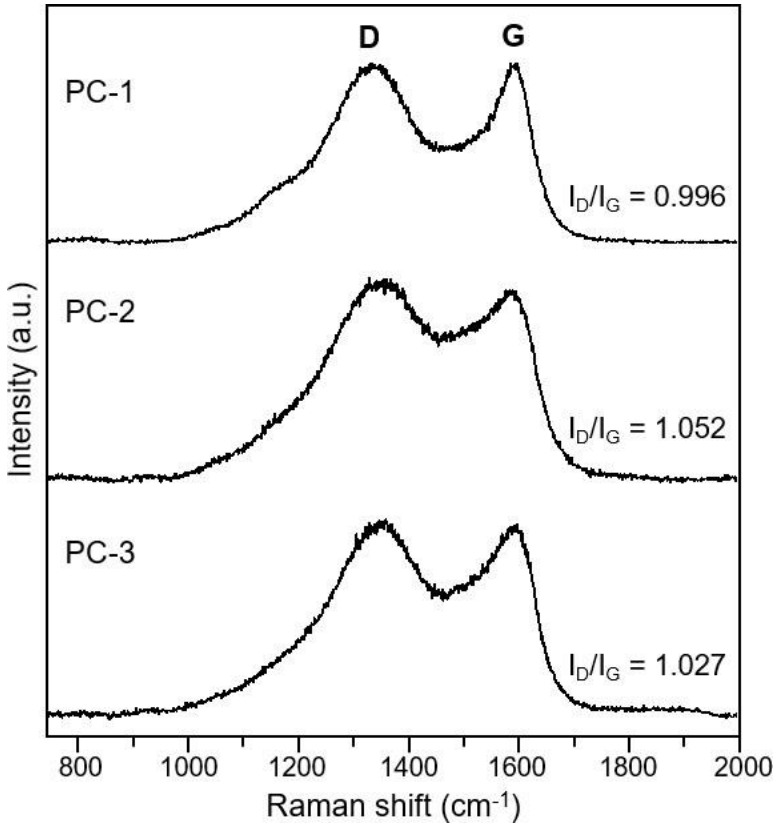

Fig. S4 Raman spectra of PC-1–PC-3.

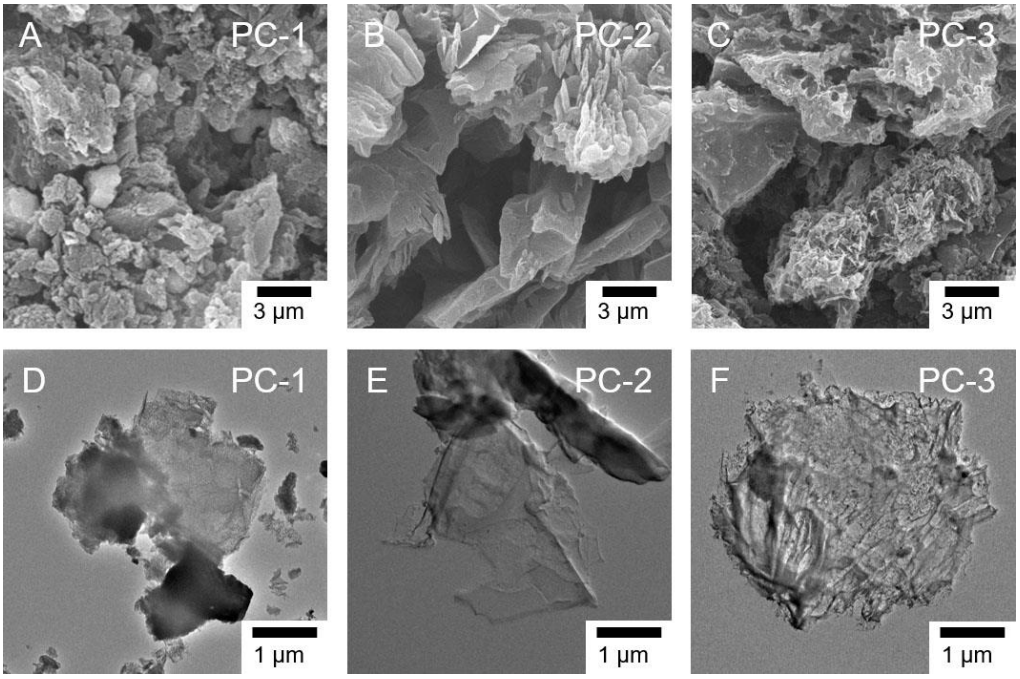

Fig. S5 (A–C) SEM and (D–F) TEM images of PC-1–PC-3.

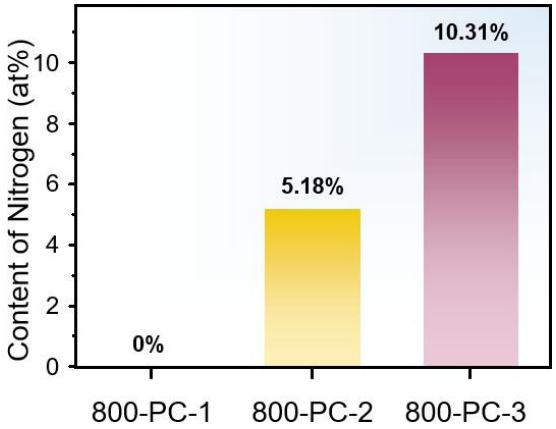

Fig. S6 Nitrogen content analysis of products (800-PC-1, 800-PC-2, and 800-PC-3) obtained after pyrolysis of MOF-5, MOF-5/urea, and MOF-5/urea@NaCl at 800 °C for 3 h.

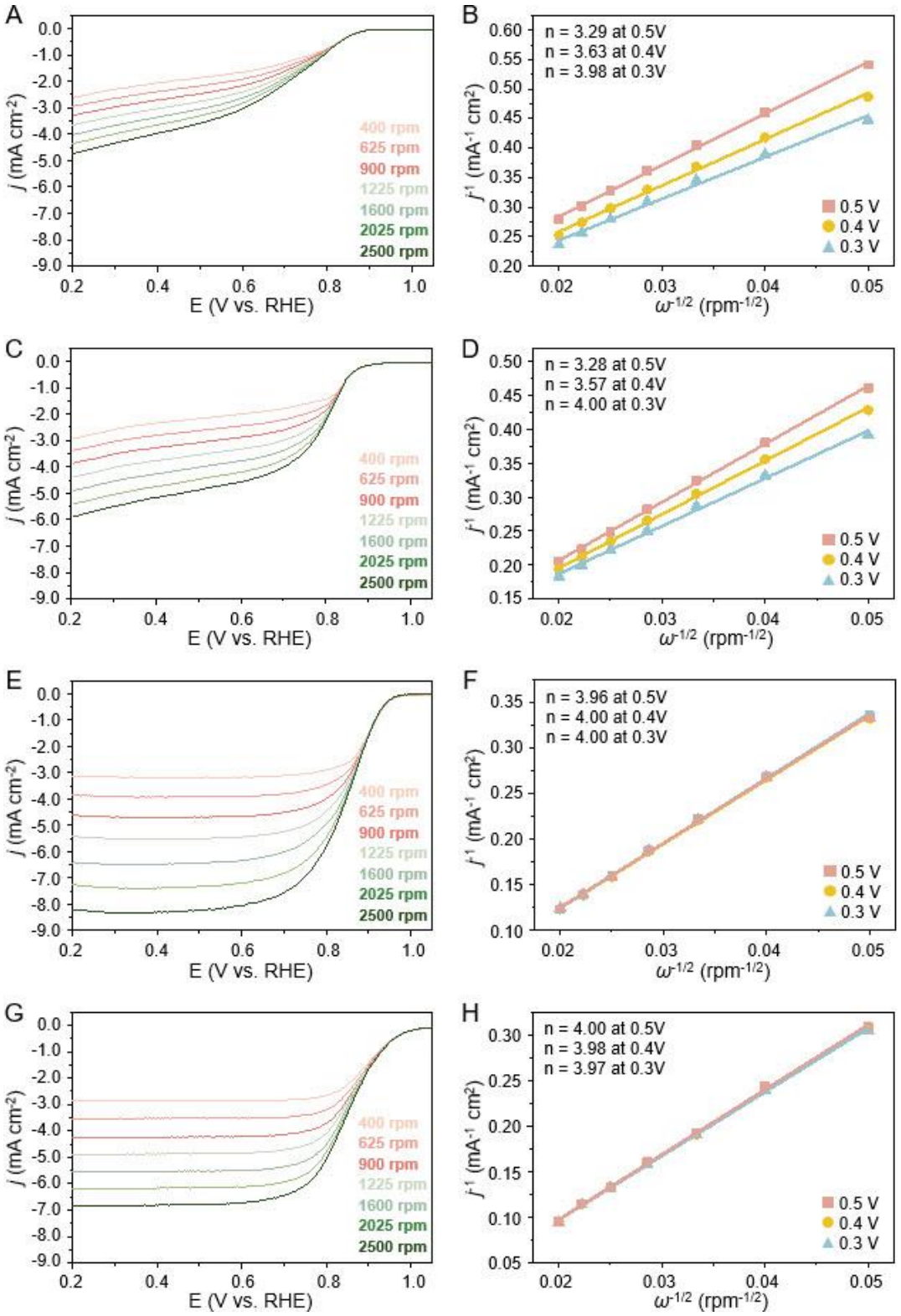

Fig. S7 (A, C, E, G) LSV curves of PC-1–PC-3 and Pt/C, respectively, recorded at different electrode rotation rates (400–2500 rpm). (B, D, F, H) K–L plots of PC-1–PC-3 and Pt/C, respectively, at various potentials (0.3–0.5 V).

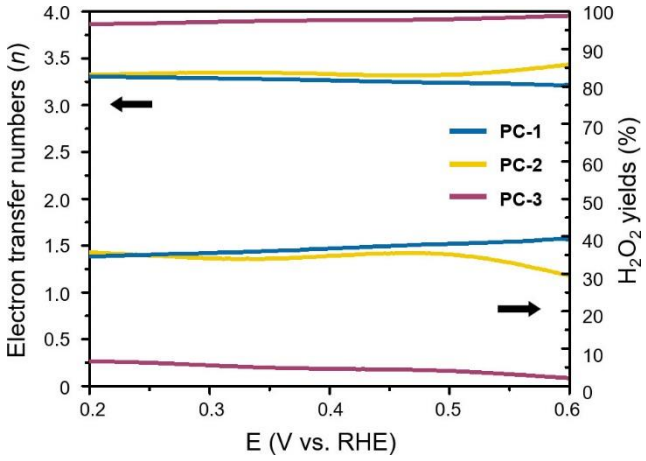

Fig. S8 Electron transfer numbers (*n*) and H_2O_2 yields of PC-1–PC-3.

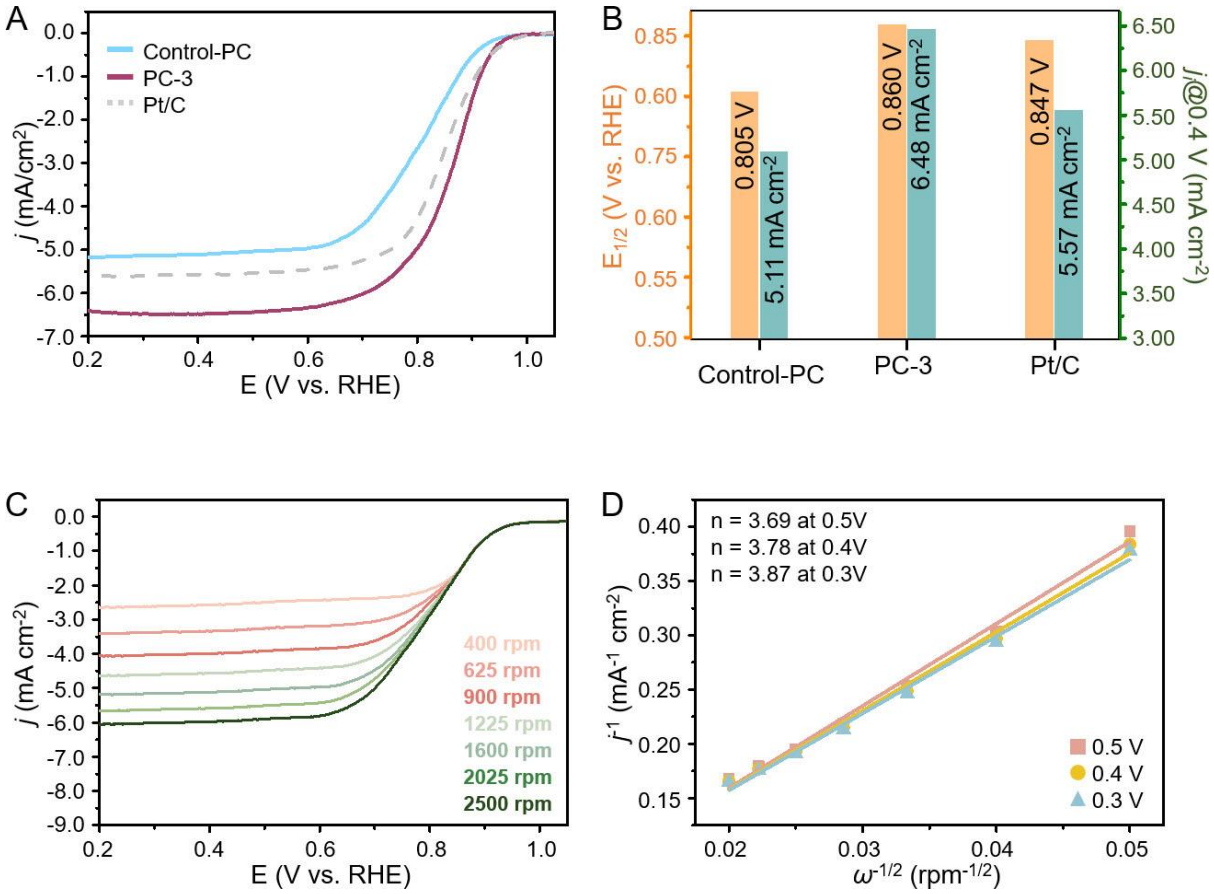

Fig. S9 (A) LSV curves of PC-3, Pt/C, and the sample derived from the MOF/urea/NaCl mixture (using NaCl as a simple additive rather than as a salt-protected shell) in O_2-saturated 0.1 M KOH electrolyte at a rotation rate of 1600 rpm. (B) Comparison of half-wave potentials and limiting current densities (j_l) at 0.4 V for catalysts. (C) LSV curves recorded at different electrode rotation rates (400–2500 rpm) and (D) K–L plots at various potentials (0.3–0.5 V) of the sample derived from the MOF/urea/NaCl mixture. The porous carbon sample derived from the MOF/urea/NaCl mixture is denoted as Control-PC.

Table S1 BET surface areas and total pore volumes of pure MOF-5 and PC-1–PC-3.

Sample	Surface area ($m^2\ g^{-1}$)	Total pore volume ($cm^3\ g^{-1}$)
MOF-5	1242	0.54
PC-1	968	0.83
PC-2	311	0.28
PC-3	1393	1.38

Table S2 Comparison of ORR activity of PC-3 with that of other electrocatalysts in the recently developed alkaline electrolyte.

Sample	Loading (mg^2 cm^{-2})	$E_{1/2}$ (V vs. RHE)	j_l (mA cm^{-2})	Reference
PC-3	0.20	0.860	6.48	This work
NBCNT-10	0.51	0.820	5.52	2
FePc@CNF	0.80	0.875	5.62	3
H-NSC@Co/NSC	0.03	0.850	5.60	4
Co/SP-NC	0.42	0.860	5.26	5
COF@ZIF-Pd_{800}	1.20	0.866	4.98	6
A-MnO_2/NSPC-2	0.29	0.870	5.40	7
$MnCo_2O_4$/NCNTs	0.20	0.760	6.06	8
C-1000	0.26	0.833	5.60	9
Porous CS	0.46	0.740	5.92	10
Cu-SACs-7	0.26	0.897	6.50	11
Co@Co_3O_4/NC-2	0.25	0.810	4.20	12
IO-$Ni_xCo_{9-x}S_8$@NSC	0.30	0.926	5.70	13
FeCo@CNTs-60	1.40	0.95	6.85	14

References

1 A. J. Graham, D. R. Allan, A. Muszkiewicz, Carole A. Morrison and S. A. Moggach, The effect of high pressure on MOF-5: guest-induced modification of pore size and content at high pressure, *Angew. Chem. Int. Ed.*, 2011, **50**, 11138–11141.

2 P. Wei, X. Li, Z. He, X. Sun, Q. Liang, Z. Wang, C. Fang, Q. Li, H. Yang, J. Han and Y. Huang, Porous N, B co-doped carbon nanotubes as efficient metal-free electrocatalysts for ORR and Zn-air batteries, *Chem. Eng. J.*, 2021, **422**, 130134.

3 Y. Wu, J. Liu, Q. Sun, J. Chen, X. Zhu, R. Abazaria and J. Qian, Molecular catalyst of Fe phthalocyanine loaded into In-based MOF-derived defective carbon nanoflowers for oxygen reduction, *Chem. Eng. J.*, 2024, **483**, 149243.

4 W. Li, J. Wang, J. Chen, K. Chen, Z. Wen and A. Huang, Core–shell carbon-based bifunctional electrocatalysts derived from COF@MOF hybrid for advanced rechargeable Zn–air batteries, *Small*, 2022, **18**, 2202018.

5 H. Chang, X. Liu, S. Zhao, Z. Liu, R. Lv, Q. Zhang and T.-F. Yi, Self-assembled 3D N/P/S-tridoped carbon nanoflower with highly branched carbon nanotubes as efficient bifunctional oxygen electrocatalyst toward high-performance rechargeable Zn-air batteries, *Adv. Funct. Mater.*, 2024, **34**, 2313491.

6 S. Fei, Z. He, S. Yang, J. Li, X. Li, H. Zhao, Q. Xu, X. Liu and Z. Jiang, In situ construction of highly dispersed Pd on cobalt nanoparticle on hollow functional cubic graphene by double framework for ORR, *Small*, 2024, **20**, 2403655.

7 L. Huo, M. Lv, M. Li, X. Ni, J. Guan, J. Liu, S. Mei, Y. Yang, M. Zhu, Q. Feng, P. Geng, J. Hou, N. Huang, W. Liu, X. Y. Kong, Y. Zheng and L. Ye, Amorphous MnO_2 lamellae encapsulated covalent triazine polymer-derived multi-heteroatoms-doped carbon for ORR/OER bifunctional electrocatalysis, *Adv. Mater.*, 2024, **36**, 2312868.

8 Z. Wang, J. Huang, L. Wang, Y. Liu, W. Liu, S. Zhao and Z.-Q. Liu, Cation-tuning induced d-band center modulation on Co-based spinel oxide for oxygen reduction/evolution reaction, *Angew. Chem. Int. Ed.*, 2022, **61**, e202114696.

9 F. Qin, P. Zuo, N. Li, S. Qu and W. Shen, 3D flower-like carbon spheres with hierarchical pore structure: an efficient asphaltene-based metal-free catalyst for ORR, *Adv. Mater. Interfaces*, 2022, **9**, 2201157.

10 C. Su, Y. Liu, Z. Luo, J.-P. Veder, Y. Zhong, S. P. Jiang and Z. Shao, Defects-rich porous carbon microspheres as green electrocatalysts for efficient and stable oxygen-reduction reaction over a wide range of pH values, *Chem. Eng. J.*, 2021, **406**, 126883.

11 X. Yao, Y. Zhu, T. Xia, Z. Han, C. Du, L. Yang, J. Tian, X. Ma, J. Hou and C. Cao, Tuning carbon defect in copper single-atom catalysts for efficient oxygen reduction, *Small*, 2023, **19**, 2301075.

12 C. Qi, L. Zhang, G. Xu, Z. Sun, A. Zhao and D. Jia, Co@Co_3O_4 nanoparticle embedded nitrogen-doped carbon architectures as efficient bicatalysts for oxygen reduction and evolution reactions, *Appl. Surf. Sci.*, 2018, **427**, 319–327.

13 Y. Son, K. Min, S. Cheong, B. Lee, S. E. Shim and S.-H. Baeck, Innovative air cathode with Ni-doped cobalt sulfide in highly ordered macroporous carbon matrix for rechargeable Zn–air battery, *Adv. Sci.*, 2024, **11**, 2407915.

14 C. Fang, X. Tang and Q. Yi, Adding Fe/dicyandiamide to Co-MOF to greatly improve its ORR/OER bifunctional electrocatalytic activity, *Appl. Catal. B Environ.*, 2024, **341**, 123346.